



Analytical Solution for a 3D Model of the Airflow in a Human Upper Respiratory Tract

Chatvarin Tasawang and Supachara Kongnuan¹

Department of Mathematics and Statistics,
Faculty of Science and Technology,
Thammasat University, Rangsit Center,
KlongLuang, Phatum Thani, 12121, Thailand
e-mail : chatvarin.ts@gmail.com (C. Tasawang)
supachara@mathstat.sci.tu.ac.th (S. Kongnuan)

Abstract : Understanding the airflow characteristics in the human respiratory tract is an important factor for treating a variety of respiratory diseases. This paper aims to demonstrate the behaviour of airflow in a human upper respiratory tract. The behaviour of airflow is described by a three-dimensional mathematical model under the assumptions that the airflow is axially symmetric flow and driven by the oscillating pressure gradient within the pulmonary. The proposed model composes of Navier-Stokes equations and the continuity equation. In this paper, we propose a method of analytical solution based on the Fourier-Bessel series form for the airflow field in the proposed model. The obtained solution of the airflow field is simulated on a three-dimensional geometry of a human respiratory tract. The results, both magnitude, and direction of the airflow characteristics show a good agreement to the fact of the airflow behaviour in the human airway and the previous research works.

Keywords : human upper respiratory; three-dimensional mathematical model; Navier-Stokes equations; analytical solution; Fourier-Bessel series.

2010 Mathematics Subject Classification : 47H09; 47H10.

1 Introduction

Although many respiratory diseases can not be cured, there are treatments to relieve or prevent relapses of their symptoms. The Aerosol drug delivery is the

¹Corresponding author.

most effective treatment of these diseases by using an inhaler; a medical device used for delivering medication into the respiratory tract [1]. By this treatment, the drug particles are directly diffused in respiratory position to relieve their symptoms. Currently, many researchers have paid attention and tried a lot to learn about how to control the transmission and the target position of drug particles inside the human airway, they have implemented various methods [2]. Some of the researchers in the field of biomedical engineering focus to develop technologies for the inhalers that lead to more effective treatment. However, understanding of the airflow characteristics in the human respiratory tract is also a very important factor for treating respiratory diseases that we should pay more attention as well.

Among many factors in the transportation of drug particles, the airflow is an important factor that defines particle trajectories and final particle locations [3]. The characteristic of the airflow and particle deposition can be studied by experimental method and mathematical modelling method. However, the experimental studies take a lot of time and high-performance computers in laboratory experiments, while the mathematical modeling takes less. By the mathematical modeling method, most of the researchers tend to express the airflow velocity by finding a solution to the Navier-Stokes equations and then simulate the airflow field. Many researchers, for instance, [4–7] presented methods of numerical solution and simulation of airflow in various position of a human airway with computational software. However, for saving computing resources and for the flow in some special conditions, there are some researchers tried to find a solution to those equations in an analytical method instead. Some works [8–12] presented an analytical solution of the Navier-Stokes equations in two dimensions by using different techniques and flow conditions. Besides, some researchers have presented methods for the analytical solution of the three-dimensional Navier-Stokes equations [13–16]. Moreover, in the study of the airflow inside the human airway, there are two types of Geometrical model construction; approximate modelling and accurate modelling. For the approximate modeling, a complexity of airway geometry is approximated by a simplified geometry so that the methods for the analytical solution can be applied.

Nevertheless, analytical expressions for the solution of airflow in the human upper respiratory tract have been founded only in [12] and [13]. In the first work [12], S. Kongnuan and J. Pholuang presented an analytical method for a two-dimensional model. Moreover, in [13], C. Tasawang and S. Kongnuan proposed the three-dimensional model of a human upper respiratory tract which covers oral cavity through the end of trachea but they presented analytical solution and simulation only for the oral cavity area. In this paper, for a complete simulation, we present an analytical expression for the solution of the airflow velocity and simulate the airflow field for the whole part of the respiratory tract in a three-dimensional geometry model. Our model is derived by applying the 3D-model structure and the conditions for the airflow presented by [12] and [13].

2 Construction of the Model

2.1 Computational Domain

Even, in reality, the geometry of the human upper respiratory tract is extremely complex as shown in Figure 1(A), but here we study the airflow behaviour while a patient uses an inhaler to deliver medication into the respiratory tract. It means that at that time the oral is opened wide, the inside of the oral cavity seems like an ellipsoid tube shape and connects to the trachea tube straight down, we can simplify the computational domain. Therefore, the approximated 3D-computational model is started from the beginning of the oral cavity and ceased at the end of the trachea as shown in Figure 1(B). It is generated from the parameters in Table 1 [12] and [13].

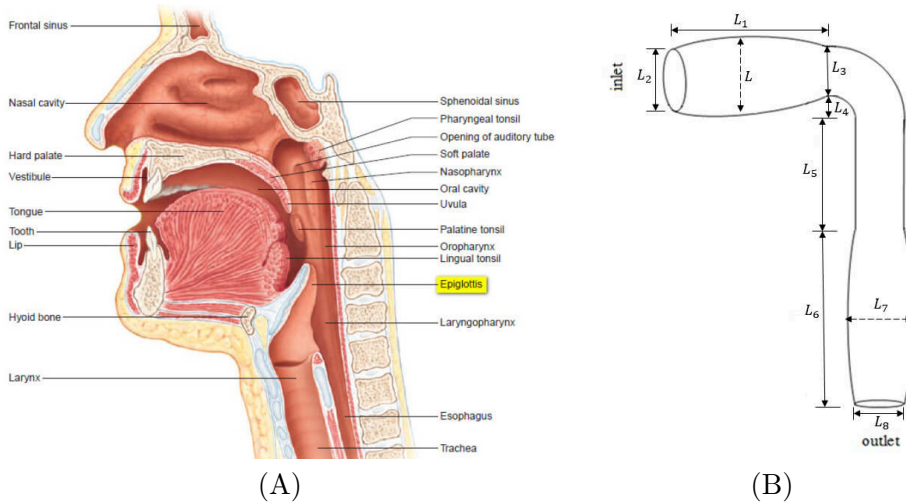


Figure 1: (A) An upper respiratory tract anatomy (Image source: Hole's Essentials of Human Anatomy and Physiology) and (B) A 3D-construction of an upper respiratory tract model

Table 1: Parameters of the upper respiratory tract.

Parameter	Length(cm)
The widest of the oral cavity, L	4.0
The length of the oral cavity, L_1	7.0
The diameter of the inlet, L_2	3.125
The diameter of pharynx, L_3	2.5
The length of the joint between the oral cavity and trachea, L_4	1.5
The length of the upper trachea, L_5	7.0
The length of the lower trachea, L_6	9.0
The widest of the lower trachea, L_7	3.25
The diameter of the outlet, L_8	2.5

2.2 Governing Equations and Boundary Conditions

In this work, we study the airflow in a simplified upper airway tube under the following assumptions as: 1) the air is homogeneous and incompressible Newtonian fluid 2) the airflow is driven by the oscillating pressure gradient and there is no effect from any external force 3) the airflow is an axial symmetric flow. The governing equations that describe the airflow are the Navier-Stokes equations and the continuity equation in the cartesian coordinate system (x, y, z) . These equations can be expressed as the following form.

$$\frac{\partial u_x}{\partial x} + \frac{\partial u_y}{\partial y} + \frac{\partial u_z}{\partial z} = 0, \tag{2.1}$$

$$\rho \left(\frac{\partial u_x}{\partial t} + u_x \frac{\partial u_x}{\partial x} + u_y \frac{\partial u_x}{\partial y} + u_z \frac{\partial u_x}{\partial z} \right) = -\frac{\partial p}{\partial x} + \mu \left(\frac{\partial^2 u_x}{\partial x^2} + \frac{\partial^2 u_x}{\partial y^2} + \frac{\partial^2 u_x}{\partial z^2} \right), \tag{2.2}$$

$$\rho \left(\frac{\partial u_y}{\partial t} + u_x \frac{\partial u_y}{\partial x} + u_y \frac{\partial u_y}{\partial y} + u_z \frac{\partial u_y}{\partial z} \right) = -\frac{\partial p}{\partial y} + \mu \left(\frac{\partial^2 u_y}{\partial x^2} + \frac{\partial^2 u_y}{\partial y^2} + \frac{\partial^2 u_y}{\partial z^2} \right), \tag{2.3}$$

$$\rho \left(\frac{\partial u_z}{\partial t} + u_x \frac{\partial u_z}{\partial x} + u_y \frac{\partial u_z}{\partial y} + u_z \frac{\partial u_z}{\partial z} \right) = -\frac{\partial p}{\partial z} + \mu \left(\frac{\partial^2 u_z}{\partial x^2} + \frac{\partial^2 u_z}{\partial y^2} + \frac{\partial^2 u_z}{\partial z^2} \right) \tag{2.4}$$

where u_x, u_y and u_z are the velocity components in the directions x, y and z respectively, p is the pressure, ρ and μ are the density and dynamic viscosity of the air, respectively.

For the boundary conditions, we define as follows: The non-slip boundary condition, $\mathbf{u} = (u_x, u_y, u_z) = (0, 0, 0)$ is assigned on the inner walls. At the inlet, the pressure is zero when compare to the outside. At the outlet, the pressure is an oscillating function sine of time, $p(t) = -P\sin(\omega t)$, where P is the amplitude of the oscillating pressure [12, 13], taken from the graph of the intrapulmonary pressure as shown in Figure 2(B(a)). Now, we have a boundary value problem (BVP) which we need to solve in the next step.

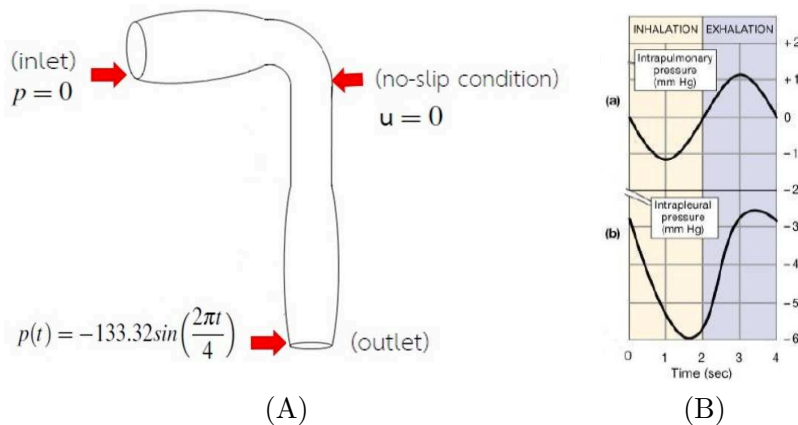


Figure 2: (A) Boundary setting and (B) graphs of (a) intrapulmonary and (b) intrapleural pressure(modified from [15])

3 The Method of Analytical Solution

From the BVP as stated in the previous section, we now want to solve for the airflow velocity and the pressure inside the computational domain. For convenience to derive an analytical expression of the airflow velocity, we divide the 3D-respiratory tract model into 4 subregions as shown in Figure 3. These subregions have their shape looked like 3 types of tube. Therefore, we divide the method of analytical solution into 3 parts as follows. However, the method for solving the third type of the subregions; area 3 and area 4, is very similar to the first region, it just alternate between x and z direction, we then omit to give the detail of finding their solution. The process of finding a solution for each subregion, we must convert the model from the cartesian coordinate system into the other coordinates that correspond to the characteristics of each area; cylindrical coordinate system and toroidal coordinate system.

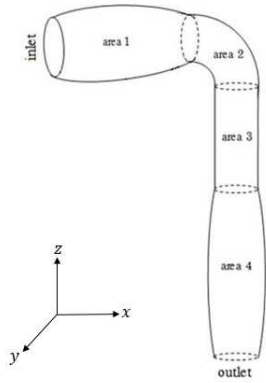


Figure 3: Division of the computational domain

Solution for the first region: area 1

The first region, area 1, we mean the oral cavity, it seems like a horizontal ellipsoid tube with circular cross section area as shown in Figure 4. We can transform the original model into the cylindrical coordinate system [12].

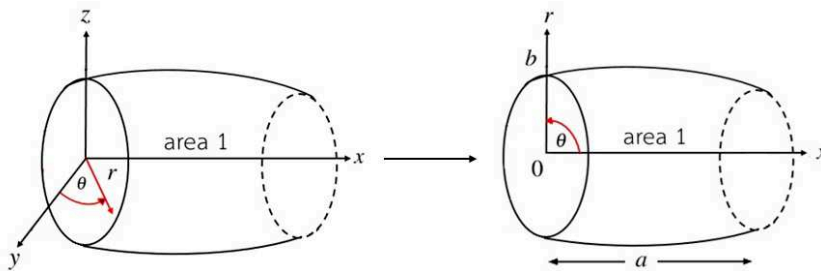


Figure 4: Transformation of area 1 into cylindrical coordinates

The left side of Figure 4 is the original geometry model in the cartesian coordinate system and the right side of Figure 4 is the model in the cylindrical coordinate system. To find an analytical solution for the airflow velocity in this area, we convert equations (2.1)-(2.4) into the cylindrical coordinate system (r, θ, x) by defining $x = x$, $y = r\cos(\theta)$, $z = r\sin(\theta)$ and use the chain rule. Then, the equations (2.1)-(2.4) become the governing equations in then cylindrical coordinates with the velocity vector $\mathbf{u} = (u_r, u_\theta, u_x)$ where u_r , u_θ , u_x are the velocity components in the directions r , θ , and x respectively.

But the airflow is assumed to be an axially symmetric flow, the angular velocity component u_θ is set to zero and $\mathbf{u} = \mathbf{u}(r, x, t)$. Therefore, these equations for the case of axially symmetric flow in cylindrical coordinates can be written in the form:

$$\frac{\partial u_r}{\partial r} + \frac{1}{r}u_r + \frac{\partial u_x}{\partial x} = 0, \quad (3.1)$$

$$\rho \left(\frac{\partial u_r}{\partial t} + u_r \frac{\partial u_r}{\partial r} + u_x \frac{\partial u_r}{\partial x} \right) = -\frac{\partial p}{\partial r} + \mu \left[\frac{\partial^2 u_r}{\partial r^2} + \frac{1}{r} \frac{\partial u_r}{\partial r} - \frac{u_r}{r^2} + \frac{\partial^2 u_r}{\partial x^2} \right], \quad (3.2)$$

$$\rho \left(\frac{\partial u_x}{\partial t} + u_r \frac{\partial u_x}{\partial r} + u_x \frac{\partial u_x}{\partial x} \right) = -\frac{\partial p}{\partial x} + \mu \left[\frac{\partial^2 u_x}{\partial r^2} + \frac{1}{r} \frac{\partial u_x}{\partial r} + \frac{\partial^2 u_x}{\partial x^2} \right]. \quad (3.3)$$

By assuming fully developed flow for this area, $u_r = 0$ and $u_x = u_x(r, t)$, the continuity equation is satisfied and we can omit equation (3.2). We are interested in the case of the flow due to an oscillating pressure gradient so the following differential equation should be satisfied:

$$\frac{\partial u_x}{\partial t} = -\frac{1}{\rho} \frac{\partial p}{\partial x} + \frac{\mu}{\rho} \left[\frac{\partial^2 u_x}{\partial r^2} + \frac{1}{r} \frac{\partial u_x}{\partial r} \right], \quad \frac{\partial p}{\partial x} = \frac{P}{a} \sin(\omega t), \quad (3.4)$$

where $\frac{P}{a}$ is the amplitude of the pressure gradient, a is the length on x -axis of the considered area, ω is the cyclic frequency of the oscillating pressure gradient. To define the oscillatory solution, we assume that u_x is periodic function as follow:

$$u_x(r, t) = u_s \sin(\omega t) + u_c \cos(\omega t). \quad (3.5)$$

By introducing dimensionless variables \tilde{r} , \tilde{u}_x , and α such that

$$\tilde{r} = \frac{r}{b}, \quad \tilde{u}_x = \frac{u_x}{Pb^2} \mu a, \quad \alpha = b \sqrt{\frac{\omega}{\nu}}, \quad (3.6)$$

where $b = b(x)$ is the radius on r -axis for each position x ; and α is the reduced frequency. Then this region is transformed to be a one-unit of length and radius tube as shown in Figure 5.

Equation (3.4) together with equation (3.5) are reduced to a system of non-homogeneous Helmholtz equations in one dimension [17];

$$\alpha^2 \tilde{u}_s = \frac{d^2 \tilde{u}_c}{d\tilde{r}^2} + \frac{1}{\tilde{r}} \frac{d\tilde{u}_c}{d\tilde{r}}, \quad -\alpha^2 \tilde{u}_c = -1 + \frac{d^2 \tilde{u}_s}{d\tilde{r}^2} + \frac{1}{\tilde{r}} \frac{d\tilde{u}_s}{d\tilde{r}} \quad (3.7)$$

The boundary conditions for \tilde{u}_s and \tilde{u}_c are stated as follows :

$$\tilde{u}_s(0) \in \mathbb{R}, \quad \tilde{u}_c(0) \in \mathbb{R}, \quad \tilde{u}_s(1) = 0, \quad \tilde{u}_c(1) = 0. \quad (3.8)$$

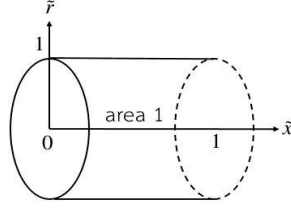


Figure 5: Dimensionless of a horizontal area

For an analytical solution of equation (3.7) which satisfies the boundary conditions (3.8), if we let $\alpha^2 \equiv \lambda^2$, we can determine by using a Fourier Bessel series of \tilde{u}_s , \tilde{u}_c for \tilde{r} . Hence, \tilde{u}_s , \tilde{u}_c and 1 are expressed [13, 18] as :

$$\begin{aligned}\tilde{u}_s &= \sum_{m=1}^{\infty} A_m J_0(\lambda_m \tilde{r}), & \tilde{u}_c &= \sum_{m=1}^{\infty} B_m J_0(\lambda_m \tilde{r}) \\ 1 &= \sum_{m=1}^{\infty} C_m J_0(\lambda_m \tilde{r}),\end{aligned}\quad (3.9)$$

where J_0 is the Bessel function of order zero which has infinite number of positive roots $\lambda = \lambda_m$; $m = 1, 2, 3, \dots$ and the term J_0 given by

$$J_0(\lambda_m \tilde{r}) = \sum_{n=0}^{\infty} \frac{(-1)^n}{(n!)^2} \left(\frac{\lambda_m \tilde{r}}{2} \right)^{2n}. \quad (3.10)$$

Substituting the series (3.9) in the system of equations (3.7), we get the unknown coefficients A_m and B_m as follows :

$$\begin{aligned}A_m &= - \left(\frac{(2n)\lambda_m^3(\lambda_m(2n-1)+1)}{\alpha^4 4n^2 + [\lambda_m^3(\lambda_m(2n-1)+1)]^2} \right) C_m, \\ B_m &= \left(\frac{\alpha^2 4n^2}{\alpha^4 4n^2 + [\lambda_m^3(\lambda_m(2n-1)+1)]^2} \right) C_m,\end{aligned}\quad (3.11)$$

where $m = 1, 2, 3, \dots$, $n = 0, 1, 2, \dots$ and we can calculate C_m by

$$C_m = \frac{\int_0^1 J_0(\lambda_m \tilde{r}) \tilde{r} d\tilde{r}}{\int_0^1 [J_0(\lambda_m \tilde{r})]^2 \tilde{r} d\tilde{r}} \quad ; m = 1, 2, 3, \dots \quad (3.12)$$

The resulting periodic velocity can be written as:

$$\tilde{u}_x = \tilde{u}_a \sin(\omega t), \quad \tilde{u}_a = \sqrt{\tilde{u}_s^2 + \tilde{u}_c^2} \quad (3.13)$$

We can obtain the airflow velocity u_x by substituting \tilde{u}_x back into equation (3.6), we get

$$u_x = \frac{Pb^2}{\mu a} \tilde{u}_x. \quad (3.14)$$

Finally, we can transform this the solution back into the cartesian coordinate form as follows: $u_x = u_x$, $u_y = u_r \cos \theta$, and $u_z = u_r \sin \theta$ which are the components of the flow velocity in x -axis, y -axis, and z -axis, respectively.

Solution for the second region: area 2

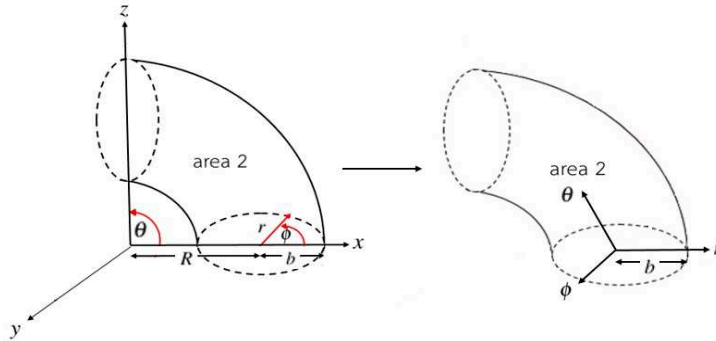


Figure 6: Transformation of area 2 into toroidal coordinates

For the curve tube, area 2, we see that it’s a quarter of a torus or the doughnut shape which the space contained within the surface to be called toroid. We will begin transform model of this area as shown in Figure 6 into the toroidal coordinate system (r, θ, ϕ) .

Similarly to the first region, we convert the equations (2.1)-(2.4) to be the equations in toroidal coordinates by defining $x = (R + r \cos \phi) \cos \theta$, $z = (R + r \cos \phi) \sin \theta$, $y = r \sin \phi$ in which $r = \sqrt{(R - \sqrt{x^2 + z^2})^2 + y^2}$, $\theta = \tan^{-1}(z/x)$, $\phi = \sin^{-1}(y/r)$. Here $\theta \in [\frac{\pi}{2}, \pi]$ is the toroidal angle, $\phi \in [0, 2\pi]$ is the poloidal angle in the tube cross section and R is the distance from the center of the tube to the center of the torus. When we use the chain rule, equations (2.1)-(2.4) become equations in toroidal coordinates with the velocity vector $\mathbf{u} = (u_r, u_\theta, u_\phi)$ where u_r, u_θ, u_ϕ are the velocity components in the directions r, θ , and ϕ respectively. By the assuming of the flow is an axially symmetric, the poloidal angular velocity component u_ϕ is set to zero and $\mathbf{u} = \mathbf{u}(r, x, t)$. Therefore, these equations in toroidal coordinates can be written in form:

$$\frac{1}{r\xi} \left(\frac{\partial}{\partial r} (r\xi u_r) + \frac{\partial}{\partial \theta} (r u_\theta) \right) = 0, \tag{3.15}$$

$$\frac{\partial u_r}{\partial t} + (\vec{u} \cdot \nabla) u_r - \frac{\cos \phi}{\xi} u_\theta^2 = -\frac{1}{\rho} \frac{\partial p}{\partial r} + \nu \left[\nabla^2 u_r - \frac{u_r}{r^2} - \frac{\cos \phi}{\xi^2} \left(u_r \cos \phi + 2 \frac{\partial u_\theta}{\partial \theta} \right) \right], \tag{3.16}$$

$$\frac{\sin \phi}{\xi} u_\theta^2 = -\frac{1}{\rho} \frac{1}{r} \frac{\partial p}{\partial \phi} + \nu \left[\frac{2}{r^2} \frac{\partial u_r}{\partial \phi} - \frac{\sin \phi}{r \xi} u_r + \frac{\sin \phi}{\xi^2} \left(u_r \cos \phi + 2 \frac{\partial u_\theta}{\partial \theta} \right) \right], \quad (3.17)$$

$$\frac{\partial u_\theta}{\partial t} + (\vec{u} \cdot \nabla) u_\theta + \frac{u_\theta}{\xi} (u_r \cos \phi) = -\frac{1}{\rho} \frac{1}{\xi} \frac{\partial p}{\partial \theta} + \nu \left[\nabla^2 u_\theta + \frac{2}{\xi^2} \left(\frac{\partial u_r}{\partial \theta} \cos \phi - \frac{u_\theta}{2} \right) \right]. \quad (3.18)$$

By assuming fully developed flow on this area, $u_r = 0$ and $u_\theta = u_\theta(r, t)$, the continuity equation as equation (3.15) is satisfied and equations (3.16)-(3.18) can be written in a new form as follows:

$$-\frac{\cos \phi}{\xi} u_\theta^2 = -\frac{1}{\rho} \frac{\partial p}{\partial r}, \quad (3.19)$$

$$\frac{\sin \phi}{\xi} u_\theta^2 = \left(-\frac{1}{\rho}\right) \left(\frac{1}{r}\right) \frac{\partial p}{\partial \phi}, \quad (3.20)$$

$$\frac{\partial u_\theta}{\partial t} = \left(-\frac{1}{\rho}\right) \left(\frac{1}{\xi}\right) \frac{\partial p}{\partial \theta} + \nu \left[\frac{1}{r \xi} \frac{\partial}{\partial r} \left(r \xi \frac{\partial u_\theta}{\partial r} \right) - \frac{u_\theta}{\xi^2} \right]. \quad (3.21)$$

Since the flow is driven by the oscillating pressure gradient which depend on the angle θ so $\frac{\partial p}{\partial r} = 0$, $\frac{\partial p}{\partial \phi} = 0$. From equation (3.19), when $u_\theta \neq 0$, we get $\cos \phi = 0$ and $\xi = R + r \cos \phi = R$. Thus, equation (3.21) becomes

$$\frac{\partial u_\theta}{\partial t} = -\frac{1}{\rho R} \frac{\partial p}{\partial \theta} + \nu \left[\frac{\partial^2 u_\theta}{\partial r^2} + \frac{1}{r} \frac{\partial u_\theta}{\partial r} - \frac{u_\theta}{R^2} \right], \quad \frac{\partial p}{\partial \theta} = \frac{P}{a} \sin(\omega t), \quad (3.22)$$

where $\frac{P}{a}$ is the amplitude of the pressure gradient, a is the width on θ of the considered area, ω is the cyclic frequency of the oscillating pressure gradient. To define the oscillatory solution, we assume that u_θ is periodic function as follow:

$$u_\theta(r, t) = u_s \sin(\omega t) + u_c \cos(\omega t). \quad (3.23)$$

By introducing dimensionless variables \tilde{r} , \tilde{u}_θ , and α such that

$$\tilde{r} = \frac{r}{b}, \quad \tilde{u}_\theta = \frac{u_\theta}{P b^2} \mu a, \quad \alpha = b \sqrt{\frac{\omega}{\nu}} \quad (3.24)$$

where $b = b(x)$ is the radius on r -axis at each point x and α is the reduced frequency. Then this region is transformed to be a one-unit region as shown in Figure 7.

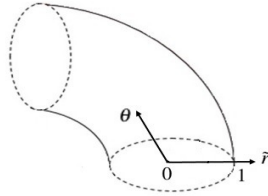


Figure 7: Dimensionless of the second region

Equation (3.23) together with equation (3.22) are reduced to a system of non-homogeneous Helmholtz equations in one dimension [17];

$$\alpha^2 \tilde{u}_s = \frac{d^2 \tilde{u}_c}{d\tilde{r}^2} + \frac{1}{\tilde{r}} \frac{d\tilde{u}_c}{d\tilde{r}} - \frac{b^2}{R^2} \tilde{u}_c, \quad -\alpha^2 \tilde{u}_c = -\frac{1}{R} + \frac{d^2 \tilde{u}_s}{d\tilde{r}^2} + \frac{1}{\tilde{r}} \frac{d\tilde{u}_s}{d\tilde{r}} - \frac{b^2}{R^2} \tilde{u}_s \quad (3.25)$$

The boundary conditions for \tilde{u}_s and \tilde{u}_c are stated as follows :

$$\tilde{u}_s(0) \in \mathbb{R}, \tilde{u}_c(0) \in \mathbb{R}, \tilde{u}_s(1) = 0, \tilde{u}_c(1) = 0. \tag{3.26}$$

Now, we let $\alpha^2 - \frac{b^2}{R^2} \equiv \lambda^2$, the analytical solution of equation (3.25) which satisfies the boundary conditions (3.26) can be determined by using a Fourier Bessel series of \tilde{u}_s, \tilde{u}_c for \tilde{r} . Hence, \tilde{u}_s, \tilde{u}_c and $\frac{1}{R}$ are expressed [18] as :

$$\begin{aligned} \tilde{u}_s &= \sum_{m=1}^{\infty} A_m J_0(\lambda_m \tilde{r}), & \tilde{u}_c &= \sum_{m=1}^{\infty} B_m J_0(\lambda_m \tilde{r}). \\ \frac{1}{R} &= \sum_{m=1}^{\infty} C_m J_0(\lambda_m \tilde{r}) \end{aligned} \tag{3.27}$$

Substituting the series (3.27) in the system of equations (3.25), we obtain the unknown coefficients A_m and B_m as follows :

$$\begin{aligned} A_m &= \left(\frac{-2nR^2(R^2(\lambda_m)^3(\lambda_m(2n-1)+1)+2nb^2)^2}{(4n^2\alpha^4R^2)+(R^2(\lambda_m)^3(\lambda_m(2n-1)+1)+2nb^2)^2} \right) C_m, \\ B_m &= \left(\frac{2nR^2(R^2(\lambda_m)^3(\lambda_m(2n-1)+1)+2nb^2)^2}{(4n^2\alpha^4R^2)+(R^2(\lambda_m)^3(\lambda_m(2n-1)+1)+2nb^2)^2} \right) C_m, \end{aligned} \tag{3.28}$$

where $m = 1, 2, 3, \dots, n = 0, 1, 2, \dots$ and we can calculate C_m by

$$C_m = \frac{\int_0^1 J_0(\lambda_m \tilde{r}) \tilde{r} d\tilde{r}}{\int_0^1 [J_0(\lambda_m \tilde{r})]^2 \tilde{r} d\tilde{r}} ; m = 1, 2, 3, \dots \tag{3.29}$$

The resulting periodic velocity can be written as :

$$\tilde{u}_\theta = \tilde{u}_a \sin(\omega t), \quad \tilde{u}_a = \sqrt{\tilde{u}_s^2 + \tilde{u}_c^2}. \tag{3.30}$$

We can obtain the airflow velocity u_θ by substituting \tilde{u}_θ back into equation (3.24). We get

$$u_\theta = \frac{Pb^2}{\mu a} \tilde{u}_\theta. \tag{3.31}$$

Finally, we can transform this the solution back into the cartesian coordinate form as follows: $u_x = u_\theta \sin(\theta), u_y = 0, u_z = -u_\theta \cos(\theta)$ which are the components of the flow velocity in x -axis, y -axis, and z -axis, respectively.

Solution for the vertical areas: area 3 and area 4

Since area 3 and area 4 are vertical ellipsoid tubes. The idea to obtain the solution for these areas is similar when we do in area 1 but for these areas, we solve for u_z instead of u_x . We omit to mention detail.

The analytical solution form of the airflow velocity of these two areas can be determined by using a Fourier Bessel series of \tilde{u}_s , \tilde{u}_c for \tilde{r} . Hence, \tilde{u}_s , \tilde{u}_c and 1 are expressed as :

$$\begin{aligned}\tilde{u}_s &= \sum_{m=1}^{\infty} A_m J_0(\lambda_m \tilde{r}), & \tilde{u}_c &= \sum_{m=1}^{\infty} B_m J_0(\lambda_m \tilde{r}) \\ 1 &= \sum_{m=1}^{\infty} C_m J_0(\lambda_m \tilde{r}),\end{aligned}\quad (3.32)$$

where J_0 is the Bessel function of order zero which have an infinite number of positive roots $\lambda = \lambda_m ; m = 1, 2, 3, \dots$ and the term J_0 given by

$$J_0(\lambda_m \tilde{r}) = \sum_{n=0}^{\infty} \frac{(-1)^n}{(n!)^2} \left(\frac{\lambda_m \tilde{r}}{2} \right)^{2n}. \quad (3.33)$$

We get the unknown coefficients A_m and B_m as follows :

$$\begin{aligned}A_m &= \left(\frac{(2n)\lambda_m^3 (\lambda_m(2n-1) + 1)}{\alpha^4 4n^2 + [\lambda_m^3 (\lambda_m(2n-1) + 1)]^2} \right) C_m, \\ B_m &= \left(\frac{-\alpha^2 4n^2}{\alpha^4 4n^2 + [\lambda_m^3 (\lambda_m(2n-1) + 1)]^2} \right) C_m\end{aligned}\quad (3.34)$$

where $m = 1, 2, 3, \dots$, $n = 0, 1, 2, \dots$ and we can calculate C_m by

$$C_m = \frac{\int_0^1 J_0(\lambda_m \tilde{r}) \tilde{r} d\tilde{r}}{\int_0^1 [J_0(\lambda_m \tilde{r})]^2 \tilde{r} d\tilde{r}} ; m = 1, 2, 3, \dots \quad (3.35)$$

The resulting periodic velocity can be written as :

$$\tilde{u}_z = \tilde{u}_a \sin(\omega t), \quad \tilde{u}_a = \sqrt{\tilde{u}_s^2 + \tilde{u}_c^2} \quad (3.36)$$

We can obtain the airflow velocity u_z by substituting \tilde{u}_z back, we get

$$u_z = \frac{Pb^2}{\mu a} \tilde{u}_z, \quad (3.37)$$

where parameter a and function b are correspondence to each area 3 and 4.

Finally, we can transform this the solution back into the cartesian coordinate form as follows: $u_x = u_r \sin(\theta)$, $u_y = u_r \cos(\theta)$, $u_z = u_z$ which are the components of the flow velocity in x -axis, y -axis, and z -axis, respectively.

4 Simulation Results and Discussion

In this study, we aim to demonstrate the behaviour of airflow in an upper respiratory tract by using our proposed mathematical model in Section 2. By the obtained analytical solution the airflow velocity based on Fourier Bessel series in Section 3, we can now simulate the vector plot and the contour plots of the airflow

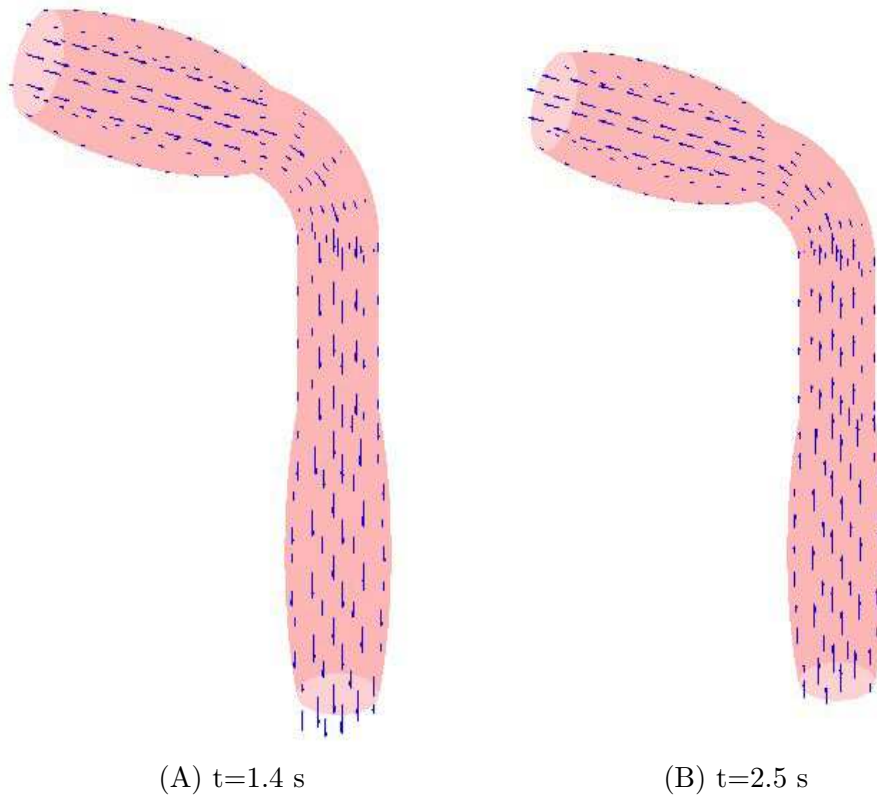


Figure 8: The 3D-arrow plot of airflow field at time $t = 1.4$ s (A) and $t = 2.5$ s (B) in a breathing period

fields in the program of Matlab R2010a. By a study of medical research [5], we found that the breathing period is assumed to be 4 s and the cyclic frequency $\omega = \frac{\pi}{2}$. The analysis is carried out with $\rho = 1.148 \text{ kg/m}^3$, $\mu = 1.82 \times 10^{-5} \text{ Pa}\cdot\text{s}$ and $P = 133.32 \text{ Pa}$. For the realistic simulation, we present the direction of airflow field by the 3D arrow plot as shown in Figure 8. The 3D-arrow plots of airflow field are demonstrated at $t = 1.4$ s and $t = 2.5$ s in a breathing period as shown in Figures 8(A)-8(B), respectively. The reason that we simulate at $t = 1.4$ s and $t = 2.5$ s is because of when $t = 1.4 \in [0, 2)$ and $t = 2.5 \in (2, 4]$ are the times that the flow should flow in because of the pulmonary relaxation and flow out because of the pulmonary contraction, respectively. From Figures 8(A)-8(B), we found that when $t = 1.4$ s the air flows into the respiratory tract, while in contrast, the air flows out the respiratory tract at $t = 2.5$ s. The results are reasonable and show a good agreement to the fact of the airflow behaviour in the human airway.

Let's see the airflow field more closer, we present the arrow plot in the XZ-plane for the central planar of respiratory tract. The XZ-plane arrow plots of velocity field at time $t = 1.4$ s, 2.05 s, 2.5 s of each breathing period are shown in Figures 9(A)-9(C).

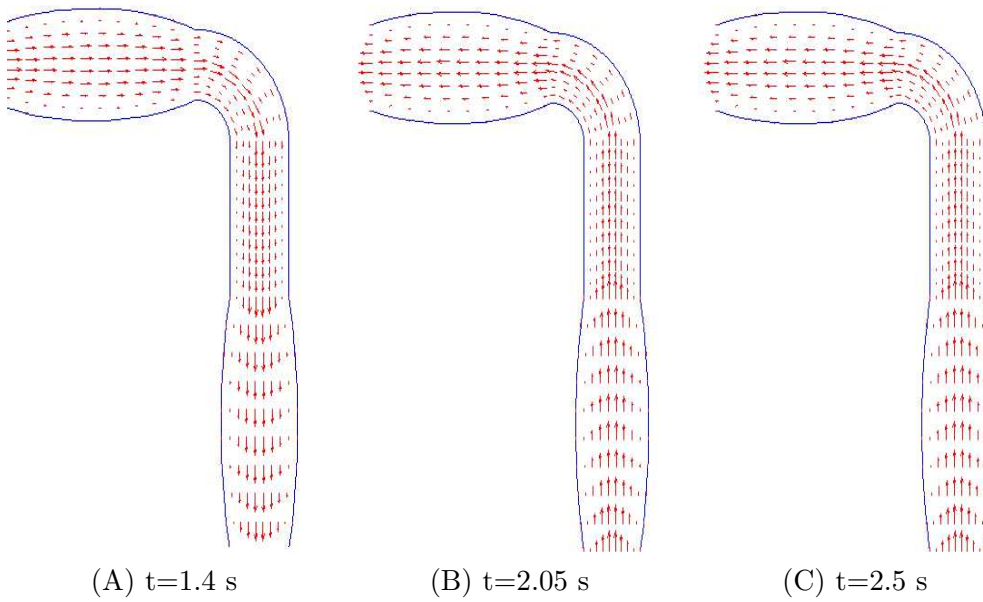


Figure 9: The XZ-plane arrow plot of airflow field at the central planar of respiratory tract at time $t = 1.4$ s (A), 2.05 s (B), 2.5 s (C) in a breathing period

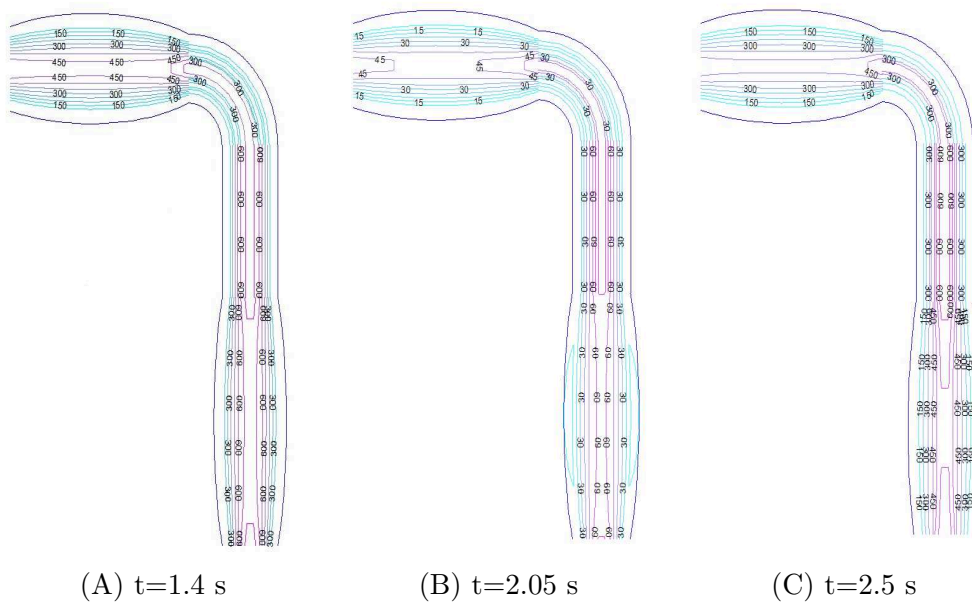


Figure 10: The XZ-plane contour plot of airflow field at the central planar of respiratory tract ($y' = 0$)

From Figures 9(A)-9(C), we see clearly that for a fixed location, the velocity profiles have different direction and different size by different time. The maximum velocity occurs in the central area and reduces to zero for the area which is more closer to the walls. The results also show agreements to pulmonary system that when $t = 1.4$ s the air flows into the respiratory tract and when $t = 2.05$ s, 2.5 s the air flows out the respiratory tract.

Additionally, we present magnitude of the airflow velocity by the contour plot in the XZ-plane for the central planar of respiratory tract at breathing period $t = 1.4$ s, 2.05 , 2.5 s as shown in Figures 10(A)-10(C), respectively. When we consider the magnitude of velocity at $t = 1.4$ s and $t = 2.5$ s, it is found that a boundary layer behaviour with a high velocity gradient close to the boundaries. The magnitude of velocity always shows the maximum value in the central area and gradually decreases to zero when the area approaching the to the walls. this results corresponds to the previous arrow plots. The maximum velocity occurs at the upper and end trachea which value have about 600 cm/s. However, when $t = 2.05$ s the direction of the airflow is changing to become the out flow, their magnitudes of velocity are less than other times and close to zero.

Moreover, we can see that at the same location, both direction and magnitude of the airflow has changed vary on time in a breathing period. The air is taken in and passing through oral cavity and enters trachea on the first two seconds of a period and changes to flow out from the trachea and pass through oral cavity on the last two seconds of the period. The obtained values of velocities are in the range of $[0, 900]$ cm/s which agree to other previous works [5,12] and [13].

5 Conclusions

A three-dimensional mathematical model under the assumptions of axially symmetric flow and driven by the oscillating pressure gradient within the pulmonary is proposed. An analytical solution based on the Fourier-Bessel series for the airflow field in a human respiratory tract is carried out as the objective of this work. The solution of the airflow field is sophisticated to simulate on a three-dimensional geometry of a human respiratory tract. The obtained results, both magnitude and direction of the airflow are reasonable show a good agreement to the fact of the airflow behaviour in the human airway. The values of velocities are in the range of $[0, 900]$ cm/s which agree to other previous works [12,13] and [5].

Acknowledgements : The authors gratefully acknowledge the financial support provided by Thammasat University Research Fund under the TU Research Scholar. The authors would like to thank Mathematics and Statistics Department, Thammasat University for giving the facilities support to this research.

References

- [1] V.K. Srivastav, A. Kumar, S.K. Shukla, A.R. Paul, A.D. Bhatt, A. Jain, Airflow and Aerosol-Drug delivery in a CT scan based human respiratory tract with tumor using CFD, *Journal of Applied Fluid Mechanics* 7(2) (2014) 345–356.
- [2] S.B. Kharat, A.B. Deonghare, K.M. Pandey, Airflow and particle transport through human airway: A systematic Review, *Materials Science and Engineering* 225 (2017) 1–4.
- [3] H. Tang, J.Y. Tu, H.F. Li, B. Au-Hijleh, C.C. Xue, C.G. Li, Dynamic analysis of airflow features in a 3D real-anatomical geometry of the human nasal cavity, 15th Australasian Fluid Mechanics Conference, Australia 13–17 December 2004.
- [4] K. Wang, T.S. Denney, E.E. Morrison, V.J. Vodyanoy, Numerical simulation of air flow in the human nasal cavity, <http://ieeexplore.ieee.org/xpl/articleDetails.jsp,arnumber=1615757>, Retrieved November 2, 2015.
- [5] Z. Zhang, C. Kleinstreuer, Airflow structures and nano-particle deposition in a human upper airway model, *Journal of Computational Physics* 198 (2004) 178–210.
- [6] X. Qingxing, Y.L. Fong, W. Chi-Hwa, Transport and deposition of inertial aerosols in bifurcated tubes under oscillatory flow, *Chemical Engineering Science* 64 (2009) 830–846.
- [7] X.Y. Luo, J.S. Hinton, T.T. Liew, K.K. Tan, LES modeling of flow in a simple airway model, *Medical engineering Physics* 26 (2004) 403–413.
- [8] S. Tsangaris, N.W. Vlachakis, Exact solution of the Navier-Stokes equations for the oscillating flow in duct of a cross-section of right-angled isosceles triangle, *Z. Angew. Math. Phys.* 54 (2003) 1094–1100.
- [9] S. Otarod, D. Otarod, Analytical solution for Navier-Stokes equations in two dimensions for laminar incompressible flow, *Fluid Dynamics; Classical Physics*, 2006.
- [10] M.R. Mohyuddin, A.M. Siddiqui, T. Hayat, J. Siddiqui, S. Asghar, Exact solutions of time-dependent Navier-Stokes equations by Hodograph-Legendre transformation method, *Tamsui Oxford Journal of Mathematical Sciences* 24 (3) (2008) 257–268.
- [11] M. Emin, C. Erdem, An Analytical Solution of the Navier-Stokes Equation for Flow over a Moving Plate Bounded by Two Side Walls, *Journal of Mechanical Engineering* 55 (12) (2009) 749–754.
- [12] S. Kongnuan, J. Pholuang, A Fourier Series-Based Analytical Solution for the oscillating Airflow in a Human Respiratory Tract, *International Journal of Pure and Applied Mathematics* 78 (5) (2012) 721–733.

- [13] C. Tasawang, S. Kongnuan, Analytical solution of a 3D model for the airflow in a human oral cavity, *Naresuan University Journal : Science and Technology* 24 (2) (2016) 132–141.
- [14] N.W. Vlachakis, A.K. Baldoukas, Exact solution of a 3D spiral flow model for a viscous fluid in a stationary porous pipe with application to blood vessels. 3rd WSEAS International Conference on Differential Equations-Theory and Applications in Wolin-Island Poland, 2002.
- [15] H.M. John.(n.d.), APHNT: Respiratory Physiology Outlines, from: <http://facstaff.bloomu.edu/jhranitz/Courses/APHNT/Outlines/Respir>, Retrieved July 26, 2009.
- [16] A. Muriel, An exact solution of the 3-D Navier-Stokes equation, *Fluid Dynamics, Mathematical Physics*, 2010.
- [17] H. Rosu, J.L. Romeo, Ermakov approach for the one-dimensional Helmholtz Hamiltonian, *Nuovo Cimento* 114 (1999) 569–574.
- [18] M. S. Gockenbach, *Partial differential equations: analytical and numerical methods* 2nd ed., The United States of America : The Society for Industrial and Applied Mathematics, 2011.

(Received 15 June 2019)

(Accepted 24 December 2019)